Plasmon dispersion in silicon obtained by analytic continuation of the random-phase-approximation dielectric matrix

R. Daling and W. van Haeringen
Department of Physics, Eindhoven University of Technology, P.O. Box 513, 5600 MB Eindhoven, The Netherlands

B. Farid
Cavendish Laboratory, Madingley Road, Cambridge CB3 0HE, United Kingdom
(Received 23 October 1990; revised manuscript received 8 April 1991)

The plasmon dispersion in silicon has been determined along the Δ and Λ axis of the first Brillouin zone, taking local-field effects fully into account. The empirical pseudopotential method has been used to obtain the electron band structure. A very effective method of analytic continuation is employed to obtain the singular integrals involved in the calculation of the random-phase-approximation polarization matrix. Using the analytic continuation of the dielectric matrix across its branch cut, we investigate the plasmon energies and lifetimes. It is shown that the experimental observability of the theoretically obtained plasmon band gap at the L point is questionable due to an unexpectedly large lifetime of plasmons in the second band as compared with those in the first band. The obtained plasmon energies are typically 10% larger than the reported experimental values. The calculated plasmon energies display a stronger dispersion than the experimental values. Moreover, the experimentally observed anisotropy in the dispersion along the Δ and Λ axis is not reproduced by our calculations.

I. INTRODUCTION

In the quantum-mechanical many-body theory of interacting particles an important role is played by the so-called dielectric function ϵ and its inverse ϵ^{-1}; these are functions of position and time, or, alternatively, of momentum and energy, as will be the case in this work. The inverse dielectric function can, for example, be used to give an exact expression for the ground-state energy of a many-particle system including correlations (see Refs. 1 and 2). Also for the understanding of the excitation properties, which can be divided in collective and single-particle excitations, ϵ is an important quantity. In case of collective excitations ϵ is of direct importance as $\epsilon^{-1}(\mathbf{q},\omega)$ is the proportionality factor between an external field $\Phi_{\text{ext}}(\mathbf{q},\omega)$ and the internal field Φ_{int}, which is set up in the many-particle system in response to Φ_{ext},

$$\Phi_{\text{int}}(\mathbf{q},\omega)=\epsilon^{-1}(\mathbf{q},\omega)\Phi_{\text{ext}}(\mathbf{q},\omega) . \tag{1}$$

In this equation $\mathbf{q}$ is the wave vector of the fields and ω their frequency. According to Eq. (1) if at a given $\mathbf{q}$ the function $\epsilon(\mathbf{q},\omega)$ vanishes for a certain frequency $\omega(\mathbf{q})$, or alternatively if $\epsilon^{-1}(\mathbf{q},\omega)$ has a pole at this frequency, an internal field with wave vector $\mathbf{q}$ and frequency $\omega(\mathbf{q})$ can exist without a driving field. This means that the system has an excitation with wave vector $\mathbf{q}$ and frequency $\omega(\mathbf{q})$ whenever $\epsilon(\mathbf{q},\omega(\mathbf{q}))=0$. In the case of a free-electron gas this excitation corresponds to a charge oscillation with respect to the positive background, a so-called plasmon.

For the understanding of the single-particle excitations of semiconductors or insulators the dielectric properties have also turned out to be of great importance. The most successful band-structure calculations for these systems are those according to the so-called GW scheme of Hedin.[3] In these calculations the electron-electron interaction is taken into account to first order in a screened interaction W, which is obtained by screening the electron-electron Coulomb interaction V_c according to the following (symbolic) equation:

$$W=\epsilon^{-1}V_c . \tag{2}$$

Examples of this kind of calculation can be found in Refs. 4–7. Essential in these calculations is the use of a sufficiently accurate dielectric function ϵ, either by using a model[4,5,7] or by calculating it.[6]

In a solid, as in the above-mentioned band-structure calculations, the dielectric properties are actually described by a dielectric matrix instead of a single function. This is so because the full translational symmetry, present in a homogeneous system, is reduced to a discrete symmetry under translations over lattice vectors. Due to this lack of translational symmetry the momentum $\mathbf{q}$ (actually we should use $\hbar\mathbf{q}$ when speaking of momentum) is no longer a conserved quantity and the dielectric function $\epsilon(\mathbf{q},\omega)$ becomes a dielectric matrix $\epsilon_{\mathbf{K}_1\mathbf{K}_2}(\mathbf{k},\omega)$ in which $\mathbf{k}$ is a vector in the first Brillouin zone (1BZ) and in which the matrix indices $\mathbf{K}_1$ and $\mathbf{K}_2$ are reciprocal-lattice vectors. The inverse dielectric function becomes the inverse dielectric matrix. This gives rise to the so-called local-field effect (LFE), expressed in the generalization of Eq. (1) to

$$\Phi_{\text{int}}(\mathbf{k}+\mathbf{K}_1,\omega)=\sum_{\mathbf{K}_2}\epsilon^{-1}_{\mathbf{K}_1\mathbf{K}_2}(\mathbf{k},\omega)\Phi_{\text{ext}}(\mathbf{k}+\mathbf{K}_2,\omega) , \tag{3}$$

meaning that the internal field has Fourier components at wave vectors that differ reciprocal-lattice vectors from the external-field wave vector. Plasmon excitations can also exist in a solid and their energies are now given, at

each $\mathbf{k}$, by solutions $\omega(\mathbf{k})$ of (Ref. 8)

$$\det[\epsilon(\mathbf{k},\omega)]=0 \ . \tag{4}$$

Calculations of the dielectric matrix ϵ for a solid have been performed in various degrees of sophistication. In Ref. 9 an analytic calculation of ϵ is presented in which the lattice potential is treated as a perturbation on the free-electron-gas results. Calculations which take the lattice potential into full account, i.e., which use a real band structure to calculate ϵ, can be found in Refs. 10–12. Of these calculations Refs. 10 and 11 both neglect the LFE and Ref. 11 only considers the static $\omega=0$ case. Reference 12 takes the LFE into account but the calculations have been restricted to $\mathbf{k}=\mathbf{0}$.

In this paper we consider the random-phase approximation (RPA) dielectric matrix of the semiconductor Si at nonzero $\mathbf{k}$ values and at energies in the neighborhood of plasmon energies. First we present a method to calculate in a convenient way the singular 1BZ integrals appearing in the expression for the dielectric matrix. Then we show how this method enables us to solve Eq. (4) explicitly and thus to study the plasmon excitations of the system. We discuss both the energies and the lifetimes of the plasmons in the Δ and Λ directions. In spite of our rigorous treatment there are apparent discrepancies with the experimental data.

II. FORMULATION

The dielectric matrix is defined by the following equation:

$$\epsilon_{\mathbf{K}_1\mathbf{K}_2}(\mathbf{k},\omega)=\delta_{\mathbf{K}_1\mathbf{K}_2}-V_c(\mathbf{k}+\mathbf{K}_1)P_{\mathbf{K}_1\mathbf{K}_2}(\mathbf{k},\omega) \ . \tag{5}$$

The momentum representation of the Coulomb interaction is given by

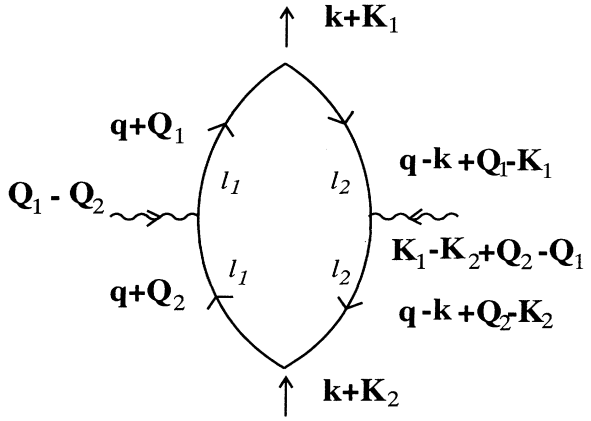

FIG. 1. Feynman diagram representing the RPA polarization matrix $P_{\mathbf{K}_1\mathbf{K}_2}(\mathbf{k},\omega)$ of a solid. The internal lines of the diagram are the electron propagators; the wiggly lines represent the interaction with the lattice, which changes the electrons momentum by a reciprocal-lattice vector. l_1 and l_2 are band indices, $\mathbf{q}$ and $\mathbf{k}$ are 1BZ vectors, and the capital letters denote reciprocal-lattice vectors.

$$V_c(\mathbf{k}+\mathbf{K}_1)=\frac{e^2}{\epsilon_0}\frac{1}{|\mathbf{k}+\mathbf{K}_1|^2} \ . \tag{6}$$

The polarization matrix $P_{\mathbf{K}_1\mathbf{K}_2}(\mathbf{k},\omega)$ appearing in Eq. (5) is taken in the RPA. The Feynman diagram representing it is shown in Fig. 1 and it is given by the following two expressions:

$$P_{\mathbf{K}_1\mathbf{K}_2}(\mathbf{k},\omega)=\frac{2}{E_v a^3}I^0_{\mathbf{K}_1\mathbf{K}_2}(\mathbf{k},\omega) \ , \tag{7}$$

in which $I_{\mathbf{K}_1\mathbf{K}_2}(\mathbf{k},\omega)$ is the dimensionless integral

$$I^0_{\mathbf{K}_1\mathbf{K}_2}(\mathbf{k},\omega)=\int_{1\mathrm{BZ}} d^3q \left[\sum_{l_1\in c}\sum_{l_2\in v}-\sum_{l_1\in v}\sum_{l_2\in c}\right]\frac{1}{\omega-\epsilon_{l_1}(\mathbf{q})+\epsilon_{l_2}(\mathbf{q}-\mathbf{k})\pm i\eta}$$
$$\times\sum_{\mathbf{Q}_2} d_{l_1\mathbf{q}}(\mathbf{Q}_2)d_{l_2\mathbf{q}-k}(\mathbf{Q}_2-\mathbf{K}_2)\sum_{\mathbf{Q}_1} d_{l_2\mathbf{q}-k}(\mathbf{Q}_1-\mathbf{K}_1)d_{l_1\mathbf{q}}(\mathbf{Q}_1) \ . \tag{8}$$

The factor 2 in Eq. (7) arises from the summation over the two possible spin values of the electron and the hole in Fig. 1; $a=5.43$ Å is the Si lattice constant and E_v is a unit of energy defined by $E_v=(2\hbar^2\pi^2)/(ma^2)=0.375$ Ry in which m is the electron mass. The $d_{l\mathbf{k}}(\mathbf{K})$ and $\epsilon_l(\mathbf{k})$ are a plane-wave coefficient and band energy, respectively. Wave vectors are in units of $(2\pi)/a$ and energies in units of E_v; $l\in c/v$ means that the summation is to be done over conduction and/or valence bands only. In the energy denominator $+i\eta$ applies if $l_1\in c$ and $l_2\in v$ and $-i\eta$ applies if $l_1\in v$ and $l_2\in c$, where η is positive and infinitesimally small. Because we have chosen the origin of our coordinate system in a bond center between two Si atoms, the plane-wave coefficients in Eq. (8) are real.

We can apply the relation

$$\frac{1}{x\pm i\eta}=P\left[\frac{1}{x}\right]\mp i\pi\delta(x) \tag{9}$$

to split $I^0_{\mathbf{K}_1\mathbf{K}_2}(\mathbf{k},\omega)$ in a real and imaginary part. The real part then becomes a principal-value integral over the 1BZ of an integrand which has singularities if $|\omega|$ exceeds the energy gap because for these ω values the energy denominator $\epsilon_{l_1}(\mathbf{q})-\epsilon_{l_2}(\mathbf{q}-\mathbf{k})$ vanishes for certain $\mathbf{q}$ values. The imaginary part is an integral of an integrand containing a δ function. This integral can be written as an integral over the surface in $\mathbf{q}$ space on which the argument of the δ function, which is the energy denominator, vanishes. These integrals are difficult to calculate. A method to obtain the imaginary part of this kind of in-

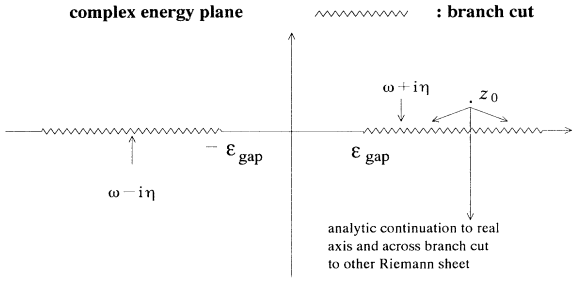

FIG. 2. Analytic structure of $\epsilon_{\mathbf{K}_1\mathbf{K}_2}(\mathbf{k},z)$ as a function of the complex variable z. z_0 is a point around which a Taylor expansion can be made in order to obtain the dielectric matrix at real energies or to obtain its analytic continuation across the branch cut. The imaginary part of z_0 has to be chosen in accordance with the $i\eta$ prescription.

tegrals can be found in Ref. 13. Once the imaginary part has been calculated the Kramers-Kronig relation can be used to obtain the real part.

If we replace the real energy variable ω in Eq. (8) by a complex variable z, the resulting function $I_{\mathbf{K}_1\mathbf{K}_2}(\mathbf{k},z)$ can be shown to be an analytic function of z with branch cuts on the real axis. One of these cuts extends from the energy gap to the highest possible one-electron–one-hole excitation energy of the system that is taken into account in Eq. (8); the other cut is obtained from the first one by reflection in $z=0$. This structure is depicted in Fig. 2. We have made use of the analyticity properties to calculate the integral in Eq. (8) in an efficient way, which we will describe in Sec. III.

First we want to discuss in more detail Eq. (4), the solutions of which were said to be the plasmon energies. In general Eq. (4) will not have real solutions, which would correspond to plasmons with an infinite lifetime. This is in contrast to what happens in a RPA calculation for the free-electron gas where $\epsilon(\mathbf{k},\omega)$ has real zeros for $|\mathbf{k}|$ values below a certain threshold. The corresponding infinite lifetime of the plasmon arises because in a uniform system it is impossible for the plasmon to decay into an electron-hole pair, the only particlelike excitation taken into account in the RPA, while at the same time obeying energy and momentum conservation. In a periodic solid the plasmon can always decay, even in the RPA, since in that case momentum has only to be conserved up to a reciprocal-lattice vector. This implies that Eq. (4) will have solutions $\omega(\mathbf{k})$ with a finite imaginary part. These solutions, however, cannot be found by searching for the zeros of $\det[\epsilon(\mathbf{k},z)]$ in which Eqs. (5)–(8) are used to evaluate the matrix elements $\epsilon_{\mathbf{K}_1\mathbf{K}_2}(\mathbf{k},z)$. Instead we have to use the analytic continuation of these elements across the above-mentioned branch cut. This can be seen by the following argument. The elements $\epsilon^{-1}_{\mathbf{K}_1\mathbf{K}_2}(\mathbf{k},z)$ of the inverse dielectric matrix can be written in a Lehmann representation (Ref. 14), which explicitly shows that they are analytic functions of z with branch cuts on the real axis. This analyticity means that if $\epsilon^{-1}_{\mathbf{K}_1\mathbf{K}_2}(\mathbf{k},z)$ has poles they will necessarily be situated on the Riemann sheets that can be reached by making the analytic continuation of $\epsilon^{-1}_{\mathbf{K}_1\mathbf{K}_2}(\mathbf{k},z)$ across the branch cut. Similar discussions concerning the location of the quasiparticle singularities in the one-particle Green's function can be found in books on many-particle theory (Refs. 15 and 16). Since singularities in $\epsilon^{-1}_{\mathbf{K}_1\mathbf{K}_2}(\mathbf{k},z)$ go together with zeros in $\det[\epsilon(\mathbf{k},z)]$ we conclude that we have to look for these zeros in the determinant of the *analytically continued* dielectric matrix.

We recall that the imaginary part of the diagonal elements of the inverse dielectric matrix can be measured in electron energy-loss experiments (Refs. 8 and 17). The probability that a fast electron exchanges momentum $\mathbf{q}$ and energy ω (actually energy $\hbar\omega$) when passing through a material is, in the Born approximation, proportional to the so-called energy-loss function $-\mathrm{Im}[\epsilon^{-1}_{\mathbf{K}\mathbf{K}}(\mathbf{k},\omega)]$ in which $\mathbf{k}$ is the unique 1BZ vector and $\mathbf{K}$ the unique reciprocal-lattice vector such that $\mathbf{k}+\mathbf{K}=\mathbf{q}$. A plasmon with momentum $\mathbf{q}=\mathbf{k}+\mathbf{K}$ will manifest itself as a resonance in $-\mathrm{Im}[\epsilon^{-1}_{\mathbf{K}\mathbf{K}}(\mathbf{k},\omega)]$; however, because of the absence of translational symmetry the momentum of a plasmon is not a good quantum number and it is therefore possible that this plasmon with momentum $\mathbf{k}+\mathbf{K}$ is also observed in $-\mathrm{Im}[\epsilon^{-1}_{00}(\mathbf{k},\omega)]$ as a second plasmon band. This is of course in complete analogy with electron band-structure theory, in which the various band energies $\epsilon_l(\mathbf{k})$ at a given $\mathbf{k}$ follow from the zeros of $\det[\omega\delta_{\mathbf{K}_1\mathbf{K}_2}-H_{\mathbf{K}_1\mathbf{K}_2}(\mathbf{k})]$, or alteratively from the poles of $[\omega\delta_{\mathbf{K}_1\mathbf{K}_2}-H_{\mathbf{K}_1\mathbf{K}_2}(\mathbf{k})]^{-1}$, the one-electron Green's function.

Whether plasmon bands in a certain direction in the 1BZ are coupled or not is purely determined by symmetry and therefore there will be no plasmon band gap above the energetically lowest-lying plasmon band in the X point of the 1BZ, whereas there will in principle be one at the L point of the 1BZ. The experimental observability of such a plasmon band gap depends on the magnitude of the coupling and on the lifetimes of the involved plasmons. We will address this problem by solving Eq. (4) explicitly.

III. METHOD OF CALCULATION

Because of the analytic structure of $I^0_{\mathbf{K}_1\mathbf{K}_2}(\mathbf{k},z)$ it is possible to use a Taylor series to represent $I^0_{\mathbf{K}_1\mathbf{K}_2}(\mathbf{k},z)$ in the neighborhood of an arbitrary complex energy z_0 which is not on a branch cut. Thus, if we want to calculate $I^0_{\mathbf{K}_1\mathbf{K}_2}(\mathbf{k},\omega)$ for real values of ω we can choose a point z_0 with a finite imaginary part in the neighborhood of the real axis and calculate the coefficients of the Taylor series around this point. These coefficients can then be used to calculate $I^0_{\mathbf{K}_1\mathbf{K}_2}(\mathbf{k},\omega)$ for real values ω not too far from z_0. We must keep in mind that the sign of ω determines the sign of the imaginary part of z_0, in order that the limit to the branch cut is taken from the appropriate side according to Eq. (8) and the discussion following it. For

positive (negative) values this means that the imaginary part of z_0 must be positive (negative) (see Fig. 2). The Taylor series of $I^0_{\mathbf{K}_1\mathbf{K}_2}(\mathbf{k},z)$ around a point z_0 has the following form:

$$I^0_{\mathbf{K}_1\mathbf{K}_2}(\mathbf{k},z)=\sum_{n=0}^{\infty} I^n_{\mathbf{K}_1\mathbf{K}_2}(\mathbf{k},z_0)(z-z_0)^n , \tag{10}$$

in which the Taylor coefficients are given by

$$I^n_{\mathbf{K}_1\mathbf{K}_2}(\mathbf{k},z_0)=\frac{1}{n!}\frac{d^n}{dz^n} I^n_{\mathbf{K}_1\mathbf{K}_2}(\mathbf{k},z)\big|_{z=z_0} \tag{11}$$

and can be obtained by differentiating the right-hand side (rhs) of Eq. (8) under the integral sign with respect to z,

$$I^n_{\mathbf{K}_1\mathbf{K}_2}(\mathbf{k},z_0)=\int_{1\mathrm{BZ}} d^3q \left[\sum_{l_1\in c}\sum_{l_2\in v}-\sum_{l_1\in v}\sum_{l_2\in c}\right]\frac{(-1)^n}{[z_0-\epsilon_{l_1}(\mathbf{q})+\epsilon_{l_2}(\mathbf{q}-\mathbf{k})]^{n+1}}$$
$$\times\sum_{\mathbf{Q}_2} d_{l_1\mathbf{q}}(\mathbf{Q}_2)d_{l_2\mathbf{q}-k}(\mathbf{Q}_2-\mathbf{K}_2)\sum_{\mathbf{Q}_1} d_{l_2\mathbf{q}-k}(\mathbf{Q}_1-\mathbf{K}_1)d_{l_1\mathbf{q}}(\mathbf{Q}_1) . \tag{12}$$

In an actual calculation the Taylor series in Eq. (10) will be truncated after a finite number (N_t) of terms.

For real ω values the representation of $I^0_{\mathbf{K}_1\mathbf{K}_2}(\mathbf{k},\omega)$ by Eqs. (10)–(12) has numerical advantages over the expression given in Eq. (8). In the first place use of the Taylor series yields both the real and the imaginary part of $I^0_{\mathbf{K}_1\mathbf{K}_2}(\mathbf{k},\omega)$ in one calculation. Second, the integrand of Eq. (12) does not have singularities because z_0 has a finite imaginary part, this as opposed to the singular integrand of Eq. (8). The third advantage of Eqs. (10)–(12) is that it is possible to evaluate the Taylor series for arguments z which lie on the other side of the branch cut as z_0; this yields the analytic continuation of $I^0_{\mathbf{K}_1\mathbf{K}_2}(\mathbf{k},z)$ across the branch cut and thus the analytic continuation of the dielectric matrix. As was argued in the preceding section, it is the analytic continuation of the dielectric matrix which we have to use in Eq. (4). The method which we have introduced here will of course work best if we apply it in a range of energy values where the functions $\epsilon_{\mathbf{K}_1\mathbf{K}_2}(\mathbf{k},\omega)$ are smoothly varying. In the neighborhood of plasmon energies this is certainly the case.

IV. RESULTS

In this section we present results of calculations that we have done according to the scheme explained above. We have calculated 15×15 dielectric matrices of Si for $\mathbf{k}$ vectors along the Δ and Λ directions in the 1BZ. In all calculations we have used 59 plane waves. The wave functions (plane-wave coefficients) and band energies have been obtained in the empirical pseudopotential scheme of which the parameters, as given in Ref. 18, are displayed in Table I. The momentum integrals in Eq. (12) have been done using the Monte Carlo method, for which the quasirandom points were generated according to the scheme described in Ref. 19.

TABLE I. Empirical pseudopotential parameters in Ry. $V_{\mathrm{epm}}(\mathbf{K})=\cos(\mathbf{K}\cdot\mathbf{t})\phi(|\mathbf{K}|)$; $\mathbf{t}=(a/8)(\hat{\mathbf{x}}+\hat{\mathbf{y}}+\hat{\mathbf{z}})$.

$\phi(\sqrt{3})$	$\phi(\sqrt{8})$	$\phi(\sqrt{11})$
-0.21	0.04	0.08

This section is divided into two parts. In Sec. IV A we discuss the convergence of our calculations with respect to parameters such as the number of integration points (N_{int}) used to calculate the integrals in Eq. (12), the number of terms N_t used in the Taylor series Eq. (10), and finally the value z_0 around which the Taylor expansion is made. In Sec. IV B we present results for the energy-loss function at various $\mathbf{k}$ values. In Sec. V we will discuss the plasmon resonances.

A. Numerical results

Figure 3 illustrates the usefulness of our method to circumvent the difficulties associated with the numerical evaluation of the principal-value integral needed to obtain the real part of Eq. (8). In this figure a comparison is made between the convergence of a numerical integration in which Eq. (8) is evaluated directly at a real energy ω and the convergence of our method to obtain the integral. In the former case the integrand has singularities in the 1BZ giving rise to the wildly fluctuating behavior of the numerical estimate as a function of the number of integration points (solid curve and dotted curve); in the

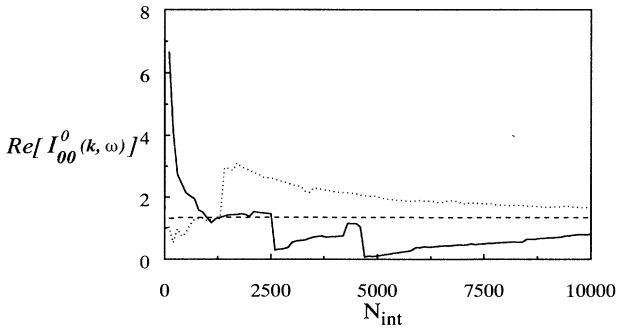

FIG. 3. Numerical estimate for the real part of $I_{00}(\mathbf{k},\omega)$ [Eq. (8)] as a function of the number of (random) integration points N_{int}; $\omega=17.85$ eV, $\mathbf{k}=(0,0.3,0.3)$. Dashed curve, tenth-order Taylor expansion around $z_0=(20.4+10.2i)$ eV according to Eq. (10); dotted curve, direct evaluation of Eq. (8) using the same random point set as was used in the calculation of the Taylor coefficient leading to the dashed curve; solid curve, same as dotted curve, but with another random point set.

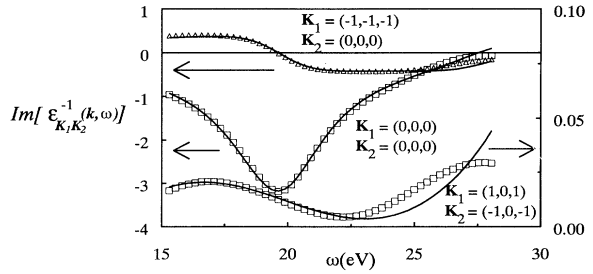

FIG. 4. Convergence of results for $\mathrm{Im}[\epsilon^{-1}_{\mathbf{K}_1\mathbf{K}_2}(\mathbf{k},\omega)]$ at $\mathbf{k}=(0,0.3,0.3)$ for three $\mathbf{K}_1,\mathbf{K}_2$ combinations. The solid lines are the results of calculations in which $\mathrm{Im}[\epsilon^{-1}_{\mathbf{K}_1\mathbf{K}_2}(\mathbf{k},\omega)]$ at $\mathbf{k}=(0,0.3,0.3)$ for three $\mathbf{K}_1,\mathbf{K}_2$ combinations. The solid lines are the results of calculations in which $z_0=(20.4+10.2i)$ eV, $N_{\mathrm{int}}=500$, and $N_t=10$ have been used. The symbols □ and △ are the result of a calculation with $z_0=(20.4+5.1i)$ eV, $N_{\mathrm{int}}=1000$, and $N_t=5$.

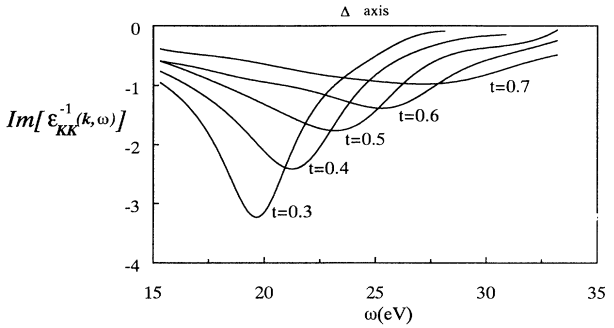

FIG. 5. $\mathrm{Im}[\epsilon^{-1}_{\mathbf{K}\mathbf{K}}(\mathbf{k},\omega)]$ for $\mathbf{q}=\mathbf{k}+\mathbf{K}=(0,t,t)$ on the Δ axis. As explained in the main text, the curves with $t\leq\frac{1}{2}$ correspond to $\mathrm{Im}[\epsilon^{-1}_{00}(\mathbf{q},\omega)]$ and those with $t>\frac{1}{2}$ correspond to $\mathrm{Im}[\epsilon^{-1}_{\mathbf{K}_X\mathbf{K}_X}(\mathbf{k},\omega)]$ in which $\mathbf{K}_X=(0,-1,-1)$ and $\mathbf{k}=-\mathbf{q}-\mathbf{K}_X$.

latter case these singularities are not present and the convergence is very much faster (dashed curve).

Figure 4 gives an idea of the numerical accuracy with which matrix elements of the inverse dielectric matrix can be obtained with our method. Of course, apart from calculating a number of integrals of the type as in Eq. (12), this also asks for an inversion of the obtained dielectric matrix. The figure shows the results of two calculations which differ in the point z_0 around which the Taylor expansion Eq. (10) is made as well as in the number of terms (N_t) taken into account in the Taylor series and in the number of integration points (N_{int}) used to evaluate the integrals. The results for the larger two elements (left scale in Fig. 4) agree over a large energy range. The energy range over which the results for a small element (right scale in Fig. 4) agree is smaller. The real parts which are not shown in Fig. 4 are obtained with a similar degree of accuracy as the imaginary parts.

Concerning the choice of the parameters in our calculations we can make the following general remark. Suppose we choose two complex energies z_0 and z_1, around which we make the Taylor expansion Eq. (10), such that z_1 has a smaller imaginary part than z_0. A smaller imaginary part causes the integrands appearing in Eq. (12) to vary more rapidly. Due to this the numerically evaluated Taylor coefficients for the expansion around z_1 are less accurate than the coefficients for the expansion around z_0 (if the same value for N_{int} is used in both calculations), an effect which will be larger for the higher-order coefficients because of the increasing power of the energy denominator. On the other hand, to obtain a reliable representation for the energy dependence of the dielectric matrix on the real axis an expansion around z_1 requires fewer terms than the expansion around z_0 because z_1 is closer to the real axis.

B. The energy-loss function

In this section we present the outcomes of calculations for $\mathbf{q}$ values along the Δ and Λ axis, corresponding to $\mathbf{q}=(0,t,t)$ and (t,t,t), respectively. In Fig. 5 $\mathrm{Im}[\epsilon^{-1}_{\mathbf{K}\mathbf{K}}(\mathbf{k},\omega)]$ is shown as a function of the energy ω for different values of $\mathbf{q}$ on the Δ axis. The curves with $t\leq\frac{1}{2}$ correspond to $\mathrm{Im}[\epsilon^{-1}_{00}(\mathbf{q},\omega)]$. For $t>\frac{1}{2}$ we actually should have calculated $\mathrm{Im}[\epsilon^{-1}_{-\mathbf{K}_X-\mathbf{K}_X}(\mathbf{q}+\mathbf{K}_X,\omega)]$ with $\mathbf{K}_X=(0,-1,-1)$. However, since $\epsilon^{-1}_{\mathbf{K}\mathbf{K}}(\mathbf{k},\omega)=\epsilon^{-1}_{-\mathbf{K}-\mathbf{K}}(-\mathbf{k},\omega)$ we can equally well calculate $\mathrm{Im}[\epsilon^{-1}_{\mathbf{K}_X\mathbf{K}_X}(\mathbf{k},\omega)]$ with $\mathbf{k}=-\mathbf{q}-\mathbf{K}_X$, so that one calculation at $\mathbf{k}=(0,t,t)$ is sufficient to obtain the energy-loss functions at both $\mathbf{q}=(0,t,t)$ and $\mathbf{q}=(=0,1-t,1-t)$. The resonance which is seen at each $\mathbf{q}$ value corresponds to a plasmon with momentum $\mathbf{q}$.

The complex zeros of $\det[\epsilon(\mathbf{k},z)]$ corresponding to these resonances are given in Table II together with the residues of the corresponding poles in the elements $\epsilon^{-1}_{\mathbf{K}\mathbf{K}}(\mathbf{k},\omega)$ with $\mathbf{K}=\mathbf{0}$ and $\mathbf{K}=\mathbf{K}_X$. Corresponding to the fact that the plasmon bands in this direction are not coupled, i.e., $\epsilon^{-1}_{\mathbf{K}_X0}(\mathbf{k},\omega)=\epsilon^{-1}_{0\mathbf{K}_X}(\mathbf{k},\omega)=0$, the zero with the

TABLE II. Zeros of the determinant of the analytically continued dielectric matrix $\epsilon(\mathbf{k},z)$ for $\mathbf{k}=(0,t,t)$. A zero of $\det[\epsilon(\mathbf{k},z)]$ gives rise to a pole in the elements $\epsilon^{-1}_{\mathbf{K}_1\mathbf{K}_2}(\mathbf{k},z)$ of the inverse-dielectric matrix. R_{00} and R_{11} are the residues of these poles in the elements $\mathbf{K}_1=\mathbf{K}_2=\mathbf{0}$ and $\mathbf{K}_1=\mathbf{K}_2=\mathbf{K}_X=[0,-1-1]$, respectively. The pole positions and residues are given in eV. The values for the zeros and residues in the first two rows at $\mathbf{k}=(0,0.3,0.3)$ have been obtained using the same two sets of parameters that were used in Fig. 4. The other zeros were calculated using a tenth-order Taylor series in Eq. (10).

t	Zero of determinant	R_{00}	R_{11}
0.3	$19.72-2.20i$	$6.22+0.69i$	0
	$19.75-2.02i$	$5.36+0.60i$	0
	$29.60-5.60i$	0	$2.09+2.65i$
0.5	$24.70-3.62i$	$3.82+4.28i$	0
	$24.50-2.70i$	0	$3.32+3.21i$

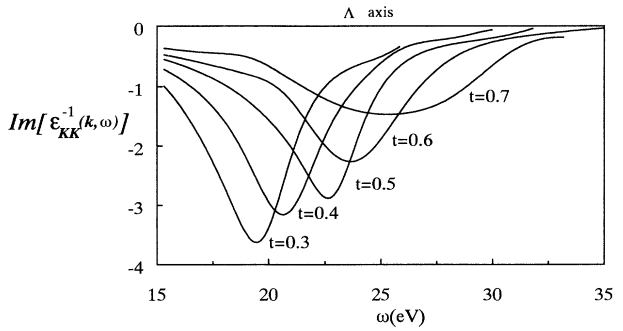

FIG. 6. $\mathrm{Im}[\epsilon^{-1}_{\mathbf{K}\mathbf{K}}(\mathbf{k},\omega)]$ for $\mathbf{q}=\mathbf{k}+\mathbf{K}=(t,t,t)$ on the Λ axis. The curves with $t \leq \frac{1}{2}$ correspond to $\mathrm{Im}[\epsilon^{-1}_{00}(\mathbf{q},\omega)]$ and those with $t > \frac{1}{2}$ correspond to $\mathrm{Im}[\epsilon^{-1}_{\mathbf{K}_L\mathbf{K}_L}(\mathbf{k},\omega)]$ in which $\mathbf{K}_L=(-1,-1,-1)$ and $\mathbf{k}=-\mathbf{q}-\mathbf{K}_L$.

larger real part does not lead to a pole in $\epsilon^{-1}_{00}(\mathbf{k},\omega)$ and conversely the zero with the smaller real part does not give a pole in $\epsilon^{-1}_{\mathbf{K}_X\mathbf{K}_X}(\mathbf{k},\omega)$. If we compare the pole parameters obtained by using two different parameter sets we find larger relative differences between them than between the functions obtained by the same two calculations. This can be seen by comparing Fig. 4 and Table II in which the two sets of pole parameters corresponding to the low-energy plasmon at $t=0.3$ (the first two rows) have been calculated with the same sets of parameters used in Fig. 4. Whereas the functions $\mathrm{Im}[\epsilon^{-1}_{00}(\mathbf{k},\omega)]$ are virtually the same, the imaginary parts of the pole positions and the real parts of the residues obtained by these two calculations differ about 10% and 20%, respectively. This difference in accuracy can be understood by the simple fact that the real axis is closer to the point z_0 around which the Taylor expansion is made than the zero of $\det[\epsilon(\mathbf{k},z)]$. Figure 6 shows $\mathrm{Im}[\epsilon^{-1}_{\mathbf{K}\mathbf{K}}(\mathbf{k},\omega)]$ for different values of $\mathbf{q}=\mathbf{k}+\mathbf{K}$ along the Λ axis.

The complex zeros of $\det[\epsilon(\mathbf{k},z)]$ are shown in Table III for three $\mathbf{k}$ values. In general the real parts of the pole positions are reasonably well determined as can be seen by comparing the results of the two calculations in which a fifth-order Taylor series and a tenth-order Taylor series were used. The imaginary parts and the residues, however, are more problematical. In agreement with the general analytic properties of the inverse dielectric matrix outlined in Sec. II all zeros of $\det[\epsilon(\mathbf{k},z)]$ shown in Tables II and III have a negative imaginary part; this is also the case for the zeros of $\det[\epsilon(\mathbf{k},z)]$ at other $\mathbf{k}$ values which are not given in Tables II and III.

V. PLASMON-DISPERSION RELATIONS

A. Theoretical results

From a purely theoretical point of view we should define the plasmon energies at a given $\mathbf{k}$ as the real part of the solutions of Eq. (4) (with ω replaced by the complex variable z),

$$\det[\epsilon(\mathbf{k},z)]=0 \ . \tag{13}$$

Another possibility to obtain plasmon energies is to calculate $-\mathrm{Im}[\epsilon^{-1}_{\mathbf{K}\mathbf{K}}(\mathbf{k},\omega)]$, and to define a clearly visible resonant structure such as a maximum or a shoulder in this quantity as a plasmon with momentum $\mathbf{q}=\mathbf{k}+\mathbf{K}$. We will call this latter definition the *experimental* definition and the former one the *theoretical* definition. In Fig. 7(a) we show the plasmon-dispersion relations along the Δ axis calculated without the LFE according to the experimental definition and with the LFE according to both the experimental and theoretical definitions. Neglecting the LFE means that the following approximation is made:

$$\epsilon^{-1}_{\mathbf{K}\mathbf{K}}(\mathbf{k},\omega)=\frac{1}{\epsilon_{\mathbf{K}\mathbf{K}}(\mathbf{k},\omega)} \ , \tag{14}$$

and that the theoretical plasmon energy at $\mathbf{q}=\mathbf{k}+\mathbf{K}$ is the real part of the solution of

$$\epsilon_{\mathbf{K}\mathbf{K}}(\mathbf{k},z)=0 \ . \tag{15}$$

The differences in plasmon energies as obtained by calculations with and without the LFE are very small for $\mathbf{q}$ values along the Δ axis; this can be made plausible by considering a 2×2 dielectric matrix involving $\mathbf{K}=\mathbf{0}$ and $\mathbf{K}=\mathbf{K}_X=(0,-1,-1)$ only, in which case there is no influence of the local field at all since the nondiagonal elements of the 2×2 matrix are zero due to symmetry, making Eq. (14) exact. Apparently the use of a larger 15×15 matrix does not make much difference.

For $\mathbf{k}$ values along the Λ axis inclusion of the LFE gives rise to essential differences between the plasmon-

TABLE III. Zeros of the determinant of the analytically continued dielectric matrix $\epsilon(\mathbf{k},z)$ for $\mathbf{k}=(t,t,t)$. A zero of $\det[\epsilon(\mathbf{k},z)]$ gives rise to a pole in the elements $\epsilon^{-1}_{\mathbf{K}_1\mathbf{K}_2}(\mathbf{k},z)$ of the inverse dielectric matrix. R_{00} and R_{11} are the residues of these poles in the elements $\mathbf{K}_1=\mathbf{K}_2=\mathbf{0}$ and $\mathbf{K}_1=\mathbf{K}_2=\mathbf{K}_L=(-1,-1,-1)$, respectively. The pole positions and residues are given in eV.

t	Zero of determinant	R_{00}	R_{11}	Zero of determinant	R_{00}	R_{11}
		Fifth-order Taylor ϵ			Tenth-order Taylor ϵ	
0.3	(19.4,−1.28)	(5.41,1.12)	(−0.38,−0.036)	(19.8,−1.89)	(5.41,2.24)	(−0.138,−0.439)
	(26.8,−4.54)	(−0.152,0.061)	(5.87,4.28)	(28.7,−4.41)	(−0.024,0.133)	(1.32,−5.20)
0.48	(22.0,−2.86)	(2.75,1.17)	(1.84,2.09)	(22.0,−3.42)	(2.50,0.143)	(2.04,5.87)
	(23.0−1.02)	(2.30,1.17)	(3.26,−0.31)	(22.8,−1.94)	(3.47,1.73)	(5.46−1.22)
0.5	(22.0,−2.81)	(2.14,1.94)	(2.40,1.33)	(21.8,−3.21)	(2.14,2.40)	(2.75,1.22)
	(23.0,−0.97)	(2.75,0.449)	(2.75,1.07)	(22.8,−1.73)	(3.98,−0.128)	(3.83,1.07)

dispersion relation according to the experimental and theoretical definition. If we do not include local-field effects in our calculation of plasmon energies according to the theoretical definition, that is, if we simply solve Eq. (15), we obtain complex energies as a function of $\mathbf{q}=\mathbf{k}+\mathbf{K}=(t,t,t)$ as displayed in Fig. 8. The solutions fall on a continuous curve. Apparently the lifetime of the "no-LFE" plasmon decreases if its energy increases. This can simply be understood by the argument that a plasmon has more possibilities to decay the larger its energy. If we include the LFE by solving Eq. (13) the complex plasmon-dispersion curve is expected to split into two separate bands. In this case it is appropriate to label the complex plasmon energies with the value of $\mathbf{k}$. At each considered $\mathbf{k}$ value we have indeed found two solutions of Eq. (13), which fall on the left and right part of the *two-branched* dotted curve in Fig. 8, respectively. As can be seen in Table III both solutions give rise to poles in $\epsilon_{00}^{-1}(\mathbf{k},z)$ as well as in $\epsilon_{\mathbf{K}_L\mathbf{K}_L}^{-1}(\mathbf{k},z)$. Obviously there are two coupled plasmon bands and the theoretical definition of the plasmon energies leads to two distinct plasmon bands with a band gap of about 1 eV in the real part.

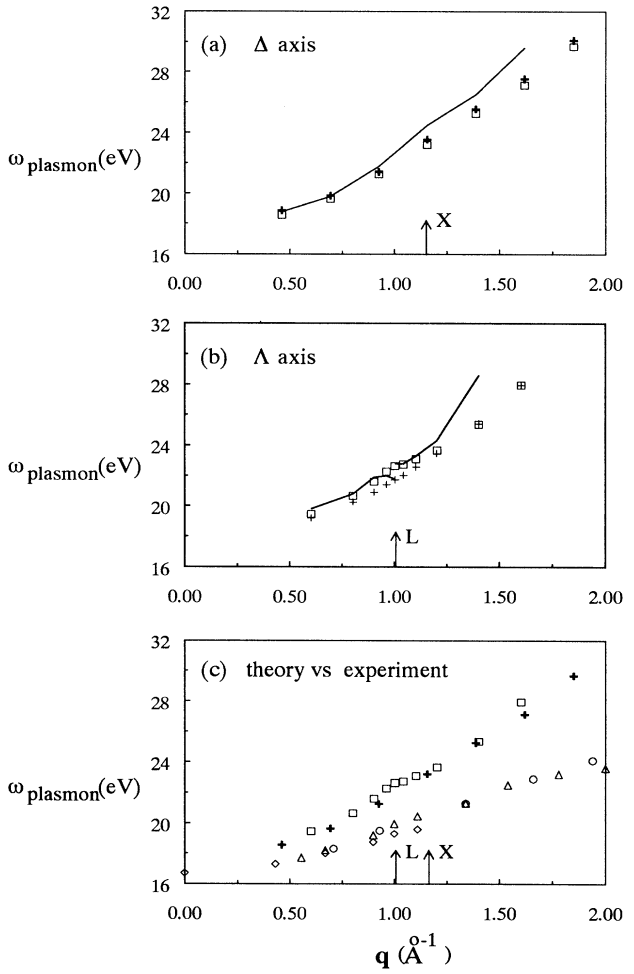

FIG. 7. Plasmon-dispersion relations. The plasmon energy at $\mathbf{q}=\mathbf{k}+\mathbf{K}$ has either been defined as the position of the maximum in $-\mathrm{Im}[\epsilon_{\mathbf{KK}}^{-1}(\mathbf{k},\omega)]$ (experimental definition) or as the real part of the zero of $\det[\epsilon(\mathbf{k},z)]$ (theoretical definition). The edges of the 1BZ in the Δ and Λ directions are marked by $\uparrow^X$ and $\uparrow^L$. (a) $\mathbf{q}$ on the Δ axis. +, no LFE's, experimental definition; □, with LFE's, experimental definition; solid curve, with LFE's, theoretical definition. (b) Same as (a), but with $\mathbf{q}$ on the Λ axis. (c) Comparison with experiment. LFE's were included in the calculation and the plasmon energies were defined according to the experimental definition. □, $\mathbf{q}$ on the Λ axis, calculated; ◇, $\mathbf{q}$ on the Λ axis, experiment (Ref. 20). +, $\mathbf{q}$ on the Δ axis, calculated; △, $\mathbf{q}$ on the Δ axis, experiment (Ref. 20); ○, $\mathbf{q}$ on the Δ axis, experiment (Ref. 21).

The real parts of the two complex plasmon bands of Fig. 8 are plotted in Fig. 7(b) as the solid line. Whether these two plasmon bands can be resolved experimentally or not will depend on the ratio of their lifetimes and on the relative strength of the poles. It turns out that if we use the experimental definition these plasmon bands cannot be resolved for $\mathbf{k}$ values near the 1BZ edge. In this connection it is important to realize that Fig. 8 shows a very remarkable feature for k values in the neighborhood of the 1BZ edge in that the lifetime of the second-band plasmon is much larger than the lifetime of the first-band plasmon. This is against the expectation one could have on the basis of the above-mentioned argument that a plasmon with larger energy has more possibilities to decay. Apparently this phase-space argument is not valid due to the local-field effects. We come back to this point further on, but the result of this peculiar difference in lifetimes is that $\mathrm{Im}[\epsilon_{00}^{-1}(\mathbf{k},\omega)]$ with $\mathbf{k}$ near the L point of the 1BZ is dominated by the second-band plasmon [the solution of Eq. (13) on the right branch of the dotted curve in Fig. 8], which manifests itself as a clear maximum in $\mathrm{Im}[\epsilon_{00}^{-1}(\mathbf{k},\omega)]$. The first-band plasmon disappears in the low-energy tail of the second-band plasmon. This is illustrated in Fig. 9 in which $\mathrm{Im}[\epsilon_{00}^{-1}(\mathbf{k}_L,\omega)]$ with $\mathbf{k}_L=(\frac{1}{2},\frac{1}{2},\frac{1}{2})$ is analyzed in its two (theoretical) plasmon contributions according to

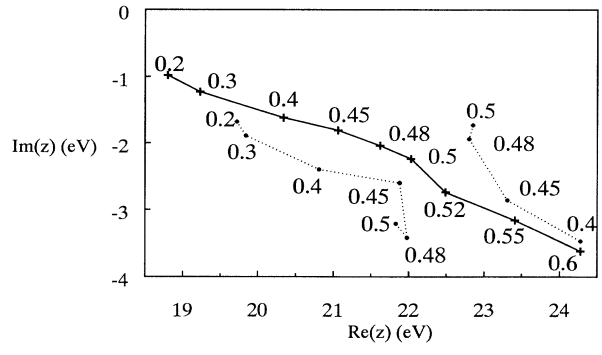

FIG. 8. Complex plasmon energies along the Λ axis. The solid curve marked with the + symbols has been obtained by disregarding the LFE; that is, by solving $\epsilon_{\mathbf{KK}}(\mathbf{k},z)=0$. The numbers along the curve denote the value of $\mathbf{q}=\mathbf{k}+\mathbf{K}=(t,t,t)$. The *two-branched* dotted curve has been obtained by including the LFE, that is, by solving $\det[\epsilon(\mathbf{k},z)]=0$. For each $\mathbf{k}=(t,t,t)$ there are two solutions, which lie on the right and left branch of the dotted curve, respectively.

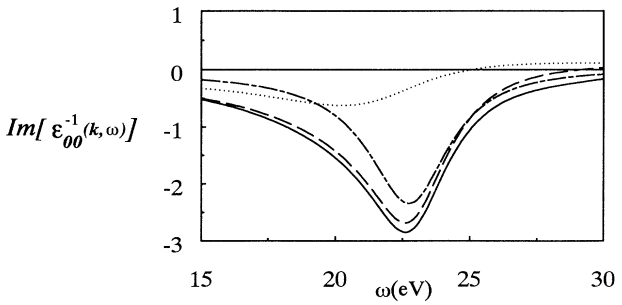

FIG. 9. Plasmon contributions to $\mathrm{Im}[\epsilon_{00}^{-1}(\mathbf{k},\omega)]$ at $\mathbf{k}=(\frac{1}{2},\frac{1}{2},\frac{1}{2})$ according to Eq. (16). The pole parameters follow from a calculation in which a tenth-order Taylor series was used and read $z_1=(21.9-3.2i)$ eV, $R_{00}^1=(2.14+2.4i)$ eV; $z_2=(22.95-1.73i)$ eV, $R_{00}^2=(3.98+0.13i)$ eV. Solid curve, $\mathrm{Im}[\epsilon_{00}^{-1}(\mathbf{k},\omega)]$; dotted curve, contribution of first-band plasmon; long-short dashed curve, contribution of second-band plasmon; dashed curve, sum of both plasmon contributions, i.e., rhs of Eq. (16).

$$\epsilon_{00}^{-1}(\mathbf{k}_L,\omega)\approx\frac{R_{00}^1}{\omega-z_1}+\frac{R_{00}^2}{\omega-z_2}\ , \tag{16}$$

in which z_1 and z_2 are the two solutions of Eq. (13) and R_{00}^1 and R_{00}^2 are the residues of the corresponding poles in $\epsilon_{00}^{-1}(\mathbf{k}_L,\omega)$.

Also for other $\mathbf{k}$ values neither $\mathrm{Im}[\epsilon_{00}^{-1}(\mathbf{k},\omega)]$ nor $\mathrm{Im}[\epsilon_{\mathbf{K}_L\mathbf{K}_L}^{-1}(\mathbf{k},\omega)]$ shows a clear double structure, which makes the experimental identification of the two, theoretically present, coupled plasmon bands difficult if not impossible.

A consequence of the large difference in lifetime is that if the experimental definition is used to define the plasmon energies it is found that these energies move continuously through the theoretical plasmon band gap as is shown in Fig. 7(b). The only remaining feature in the (experimentally defined) plasmon-dispersion relation along the Λ axis in Fig. 7(b) is a small structure at $\mathbf{q}$ values near the 1BZ edge. This structure is not present in the plasmon dispersion along the Δ axis and therefore, according to this empirical pseudopotential method (EPM) calculation, it is possible to observe experimentally the presence of two coupled plasmon bands indirectly, in spite of the above-mentioned difficulty to disentangle the energy-loss spectrum at a given $\mathbf{q}$ in its two plasmon contributions.

To show that the unexpected influence of the LFE on the lifetimes of the two plasmons near the L point of the 1BZ is not due to a too small dielectric matrix, we analyze the 2×2 dielectric matrix in this point and show that the lifetime-effect can quantitatively be understood in this 2×2 system. As before let $\mathbf{K}_L=(-1,-1,-1)$ and $\mathbf{k}_L=(\frac{1}{2},\frac{1}{2},\frac{1}{2})$. At $\mathbf{k}_L$ the following properties hold: $\epsilon_{00}(\mathbf{k}_L,z)=\epsilon_{\mathbf{K}_L\mathbf{K}_L}(\mathbf{k}_L,z)$ and $\epsilon_{0\mathbf{K}_L}(\mathbf{k}_L,z)=\epsilon_{\mathbf{K}_L0}(\mathbf{k}_L,z)$. Let the zero of $\epsilon_{00}(\mathbf{k}_L,z)$ be z_{nlf}, thus $\mathrm{Re}(z_{nlf})$ is the theoretically defined plasmon energy if local-field effects are neglected. The effect of the local field can be estimated by expanding the matrix elements around z_{nlf},

$$e_{00}(\mathbf{k}_L,z)=\epsilon_{\mathbf{K}_L\mathbf{K}_L}(\mathbf{k}_L,z)\approx a\,(z-z_{nlf})\ , \tag{17}$$

$$\epsilon_{0\mathbf{K}_L}(\mathbf{k}_L,z)=\epsilon_{\mathbf{K}_L0}(\mathbf{k}_L,z)\approx b\ . \tag{18}$$

The complex plasmon energies are then approximately given by the solutions of

$$\begin{vmatrix} a\,(z-z_{nlf}) & b \\ b & a\,(z-z_{nlf}) \end{vmatrix}=0\ , \tag{19}$$

which are

$$z_{lf}=z_{nlf}\pm\frac{b}{a}\ . \tag{20}$$

The value of b/a turns out to be $b/a=(-0.66-0.7i)$ eV. Using $z_{nlf}=(22.0-2.24i)$ eV which can be read from Fig. 8 we find the two zeros $z_{lf}=(21.34-2.94i)$ eV and $z_{lf}=(22.66-1.54i)$ eV. Indeed we see that the solution with the larger real part is closest to the real axis. These approximate plasmon energies compare very well with the plasmon energies $z_p=(21.83-3.21i)$ eV and $z_p=(22.85-1.73i)$ eV, obtained by solving Eq. (13) using a 15×15 dielectric matrix. This shows that the plasmon energies have nearly converged with respect to the dimension of the dielectric matrix and therefore the effect of the local field on the lifetimes of the plasmons is not an artifact of a too small dielectric matrix.

B. Comparison with experiment

In Fig. 7(c) a comparison is made between the experimentally determined plasmon energies[20,21] and the calculated plasmon energies. The experimental values are defined as the position of the maximum in the measured energy-loss spectrum at a given $\mathbf{q}$ and likewise the calculated values are according to the experimental definition given in Sec. V A. Our results disagree with the experimental value at three points. First, at low-$\mathbf{q}$ values the calculated plasmon energies are about 10% larger than the experimental values. Second, the calculated dispersion is stronger than the dispersion in the experimental data, which means that the discrepancy between theory and experiment becomes larger at higher-$\mathbf{q}$ values. The third point of discrepancy between our calculations and experiment is the anisotropy between the plasmon energies along the Δ and the Λ axes. Whereas in our calculations the experimentally defined plasmon energy at the L point of the 1BZ is higher than the plasmon energy at the same $\mathbf{q}$ value on the Δ axis due to the dominance of the second-band plasmon, the opposite behavior is observed in the experimental data. The first two points of disagreement are also observed in the results of Sturm.[9] However, Sturm finds the correct anisotropic behavior in the plasmon dispersion, although in his calculation the Si lattice potential has been treated perturbatively in contrast to the use of an "exact" band structure in our calculations.

The fact that the calculated plasmon dispersion is too strong must probably be ascribed to the RPA. Calcula-

tions for uniform systems which go beyond the RPA by including so-called exchange-correlation corrections in the dielectric response show that these exchange-correlation corrections do indeed flatten the plasmon dispersion.[22–24] Another cause for the observed discrepancies could be the use of the simple EPM band structure. We are presently recalculating the results presented in this paper within a local-density-approximation scheme (LDA). In this framework we will be able to incorporate static (i.e., energy independent) exchange-correlation corrections in a natural way. A further source of error in our results might be the fact that our calculations are done at zero temperature in contrast to the experimental determination of the plasmon energies which are done at room temperature.

As was argued in Sec. V A by means of the 2×2 dielectric matrix, the observed discrepancies cannot be attributed to a possibly too small dielectric matrix. In the same way the small difference between the plasmon energies along the Δ axis obtained with and without the LFE, respectively, shows that the difference in dispersion between theory and experiment at high-$\mathbf{q}$ values cannot be ascribed to the dimension of the dielectric matrix. As can be seen in Fig. 7(b), the same reasoning holds for $\mathbf{q}$ values on the Λ axis which are not close to the 1BZ edge.

VI. SUMMARY AND CONCLUSIONS

In the first part of this paper we have introduced a very effective method to calculate the type of singular integrals that often appear in the perturbation theoretic treatment of many-particle systems. These integrals have in common that the integrand contains an energy denominator which depends on an energy variable ω. For ω values exceeding some threshold value, which is zero for metallic systems but nonzero for semiconductors and insulators, these denominators may vanish for certain values of the integration variable, which makes the integrand a singular function. In our method we avoid evaluating these singular integrals by making a Taylor series around a complex energy. The calculation of the Taylor coefficients at this complex energy requires only the numerical integration of regular functions, which is much easier than the direct evaluation of the singular integrals. The method yields the real and imaginary parts of the integral in one calculation with good numerical accuracy. Moreover, it opens the possibility to investigate the analytic continuation of the integrals across the branch cuts, which they generally possess.

An example of the above-mentioned type of integrals is encountered in the calculation of the polarization matrix of a semiconductor. We have calculated the Si polarization matrix in the RPA and have used it to calculate the inverse dielectric matrix at several $\mathbf{k}$ values in the 1BZ. Using the above-mentioned possibility to obtain the analytic continuation of the dielectric matrix we have been able to investigate the $\mathbf{k}$-dependent complex plasmon energies defined as the zeros $\det[\epsilon(\mathbf{k},z)]$ [Eq. (13)]. The plasmon-dispersion relations along the Δ and Λ direction, calculated according to the experimental definition, which defines a plasmon energy as the location of the maximum in the energy-loss function, turn out to be in disagreement with the experimentally determined plasmon relations, although both band-structure effects and local-field effects were fully included. We have argued that this disagreement cannot be ascribed to the small 15×15 dielectric matrix which we have used, but is probably due to the RPA.

ACKNOWLEDGMENTS

One of us (B.F.) was supported by the Science and Engineering Research Council of the United Kingdom.

[1]P. Nozieres and D. Pines, Nuovo Cimento **9**, 470 (1958).
[2]R. Brout and P. Carruthers, *Lectures on the Many-Electron Problem* (Interscience, New York, 1963).
[3]L. Hedin, Phys. Rev. **139**, A796 (1965).
[4]M. S. Hybertsen and S. G. Louie, Phys. Rev. B **34**, 5390 (1986).
[5]W. von der Linden and P. Horsch, Phys. Rev. B **37**, 8351 (1988).
[6]R. W. Godby, M. Schlüter, and L. J. Sham, Phys. Rev. B **37**, 10 159 (1988).
[7]N. Hamada, N. Hwang, and A. J. Freeman, Phys. Rev. B **41**, 3620 (1990).
[8]W. M. Saslow and G. F. Reiter, Phys. Rev. B **7**, 2995 (1973).
[9]K. Sturm, Adv. Phys. **31**, 1 (1982).
[10]J. P. Walter and M. L. Cohen, Phys. Rev. B **5**, 3101 (1972).
[11]P. K. W. Vinsome and M. Jaros, J. Phys. C **3**, 2140 (1970).
[12]S. G. Louie, J. R. Chelikowsky, and M. L. Cohen, Phys. Rev. Lett. **34**, 155 (1975).
[13]B. Farid, D. Lenstra, and W. van Haeringen, Solid State Commun. **67**, 7 (1988).
[14]H. Lehmann, Nuovo Cimento **11**, 342 (1954).
[15]J. C. Inkson, *Many-Body Theory of Solids* (Plenum, New York, 1984).
[16]J. W. Negele and H. Orland, *Quantum Many-Particle Systems* (Addison-Wesley, Reading, MA, 1988).
[17]P. Noziéres and D. Pines, Phys. Rev. **113**, 1254 (1959).
[18]M. L. Cohen and T. K. Bergstresser, Phys. Rev. **141**, 789 (1966).
[19]J. Halton, Numer. Math. **2**, 84 (1960).
[20]J. Stiebling and H. Raether, Phys. Rev. Lett. **40**, 1293 (1978).
[21]C. H. Chen, A. E. Meixner, and B. M. Kincaid, Phys. Rev. Lett. **44**, 951 (1980).
[22]J. T. Devreese, F. Brosens, and L. F. Lemmens, Phys. Rev. B **21**, 1349 (1980); **21**, 1363 (1980).
[23]K. Utsumi and S. Ichimaru, Phys. Rev. B **23**, 3291 (1981).
[24]M. Taut, J. Phys. C **19**, 6009 (1986).